



Distribution and engulfment behavior of TiB₂ particles or clusters in wedge-shaped copper casting ingot

Jing SUN, Xiao-bo ZHANG, Qing CAI, Yi-jie ZHANG, Nai-heng MA, Hao-wei WANG

State Key Laboratory of Metal Matrix Composites, Shanghai Jiao Tong University, Shanghai 200240, China

Received 12 January 2014; accepted 6 May 2014

Abstract: Wedge-shaped copper casting experiment was conducted to study the engulfment behavior of TiB₂ particle and the interaction between particle or cluster and the solid/liquid front in commercial pure aluminum matrix. The experimental results show that the particle size distribution obeys two separate systems in the whole wedge-cast sample. Furthermore, it is found that the big clusters are pushed to the center of the wedge shaped sample and the single particle or small clusters consisting of few particles are engulfed into the α -Al in the area of the sample edge. The cluster degree of particles varies in different areas, and its value is 0.2 and 0.6 for the cluster fraction in the edge and in the center of the wedge sample, respectively. The cluster diameter does not obey the normal distribution but approximately obeys lognormal distribution in the present work. More importantly, in the whole sample, the particle size obeys two separate log-normal distributions.

Key words: discontinuously reinforced aluminum matrix composites; TiB₂; wedge-shaped copper mold casting; particle distribution; particle engulfment

1 Introduction

Discontinuously reinforced aluminum (DRA) matrix composites have been studied to improve the physical and mechanical properties for more than half a century. Although many new techniques have been developed for the fabrication of the DRA composites, such as spray deposition, powder metallurgy and several casting methods which include squeeze-casting, stir-casting and compocasting [1–4], there are still many challenges in producing the uniformly distributed DRA materials. The physical and mechanical properties were dramatically influenced by the distribution, size and shape parameters of the reinforced particles [5–7]. Among these various factors, the distribution of the ceramic particles was the most important. Generally, the size distribution of the particle or the cluster should obey normal distribution or log-normal distribution in the whole sample [8–11]. In turn, it is the interaction between the particles and the liquid/solid interface that governs the ultimate particle distribution. A wealth of available literatures showed that the pushing and engulfment behavior between the moving solid/liquid front and the particle was studied in the past decades

[12,13]. Based on the critical velocity, many models had been proposed by considering a force balance at the solidification front to predict the engulfment behavior of the particles or clusters. A common suggestion was that the critical velocity was inversely proportional to the R_p^n , where n varies from -0.1 to -3 [14–19].

UHLMANN et al [16] studied the engulfment behavior of some given particles in transparent organic matrix. Based on the surface energy, the critical velocity for particle engulfment was given as

$$v_{cr} = \frac{(n+1)}{2} \left(\frac{\Delta H_f \rho a_0 V_0 D}{kTR^2} \right) \quad (1)$$

where R is the radius of the particle; D is the diffusion coefficient; a_0 is the lattice constant; H_f is the fusion heat of the composite; ρ is the density; V_0 is the atomic volume of the solidification material; n equals 4.0–5.0; k is the Boltzmann constant and T is the temperature.

In the related literatures, BOLLING and CISCHE [17] suggested a model on the basis of the viscous drag of liquid on a particle during the solidification. The critical velocity can be calculated from

$$v_{cr} = \left[\frac{4\mathcal{P}(\alpha)kT\sigma_{SL}a_0}{9\pi\eta^2R^3} \right]^{1/2} \quad (2)$$

where η is the viscosity of the liquid; σ_{SL} is the solid/liquid interface energy; $\Psi(\alpha)$ can be calculated from the formula $\Psi(\alpha)=\alpha(1-\alpha)^2(\beta-\ln \alpha)$ and α is a constant which meets $\alpha < 1$.

According to STEFANESCU et al's work [18], the expression for the critical velocity was given by

$$v_{cr} = \frac{\Delta\sigma_0 a_0}{6(n-1)\eta R} \left[2 - \frac{K_p}{K_L} \right] \quad (3)$$

In Eq. (3), $\Delta\sigma_0$ is the surface energy difference between particles and the solidification phase; n is a constant of 2–7 [15]; K_p and K_L are the thermal conductivities of particles and the solidification phase, respectively. Detailed insight works had been conducted in latter work both by computer simulation and experiment [20–25].

In the present work, a novel phenomenon for TiB_2 particles was found: the small particles were engulfed while the big clusters were pushed during the rapid solidification process. Therefore, in this work, a wedge-shaped copper casting sample was used to study the particle distribution and the mechanism of particle engulfment correlating to different solidification rates. According to the experimental results, the mechanism about the structure of the cluster itself was discussed.

2 Experimental

The material used in the present work was pure commercial aluminum containing 10% TiB_2 particles (10% TiB_2/Al , mass fraction), which were in situ produced by mixed salts method (K_2TiF_6 and KBF_4) in appropriate proportion. The samples utilized in the experiment were produced in a standard wedge-shaped copper mold (Fig. 1). The commercial pure aluminum was melted in clay crucible placed in the resistance furnace and heated to about 750 °C. After that, the mixed salts were added into the melt to in situ produce TiB_2 and then the melt was maintained at 850 °C for about 1 h. Before pouring into the mold, the mechanical stirring was maintained to avoid the particulate segregation. To facilitate observation, the wedge-shaped sample was sectioned along a plane perpendicular to the two inclined faces of the wedge as the cooling rate decreases and the

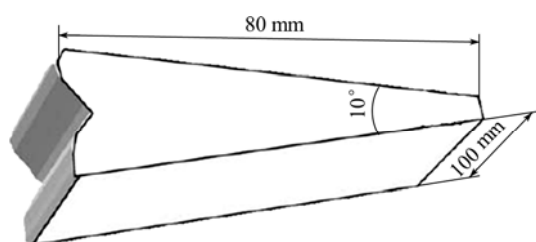


Fig. 1 Schematic diagram of wedge-shaped sample

samples were marked as samples EP1, EP2, EP3 and EP4 in the edge of the wedge sample and CP1, CP2, CP3, CP4 in the center of the wedge sample in sequence.

The samples for scanning electron microscopy observation were prepared using standard metallographic techniques and were etched using 0.5% HF solution for 3–4 min. Moreover, to gain the statistical distribution and the size of the particles in the Al matrix, the microstructure features were digitized and analyzed using image analysis software.

3 Results

3.1 Particle distribution

The solidification microstructure of the sample is shown in Fig. 2. The polarizing microstructure of the whole wedge-cast sample is shown in Fig. 2 and the dark spots are particle clusters or some pores produced in the etching process. As shown in Fig. 2, the particle distribution close to the wedge inclined surface (EP1, EP2, EP3 and EP4) is relatively uniform compared with its counterparts in the center area (CP1, CP2, CP3 and CP4). To make further study of the particle size distribution statistics in different areas of the sample, the microstructure pictures are disposed through image analysis facility and the results are shown in Fig. 3.

The statistical results indicate that in the edge of the sample, particle diameter ranges in a small scope of 0–0.6 μm , in which 80% of them are less than 100 nm and the diameter for all particles is below 600 nm. By contrast, in the center of the wedge sample, all the cluster diameter is above 1 μm and the biggest one can reach 110 μm . However, up to 90% of the clusters are distributed in the range of 1–5 μm , which is obvious in Fig. 3(c). It can be concluded that the particle or cluster size actually does not follow normal distribution while it obeys quasi log-normal distribution which is obvious in Figs. 3(a) and (b). Figure 3(d) shows that in the whole sample, the distribution of particle or cluster diameter is not subjected to an integral log-normal distribution. The diameter distributions at the edge and the center of the wedge sample are two separate systems. Therefore, it indicates that the engulfment behavior of particles in these two different areas might be processed under two different mechanisms.

According to the results, it is evident to conclude that particle area accounts for 3.3% of the total area by average in the edge of the wedge sample, which is very small compared with the value of 7.3% in the center of the sample. From samples 1 to 4, the area proportion rises with the decrease of cooling rate. Furthermore, the standard deviation of particle size is about 0.060 in the edge of the sample, indicating that the particulate size does not departure from the mean value seriously.

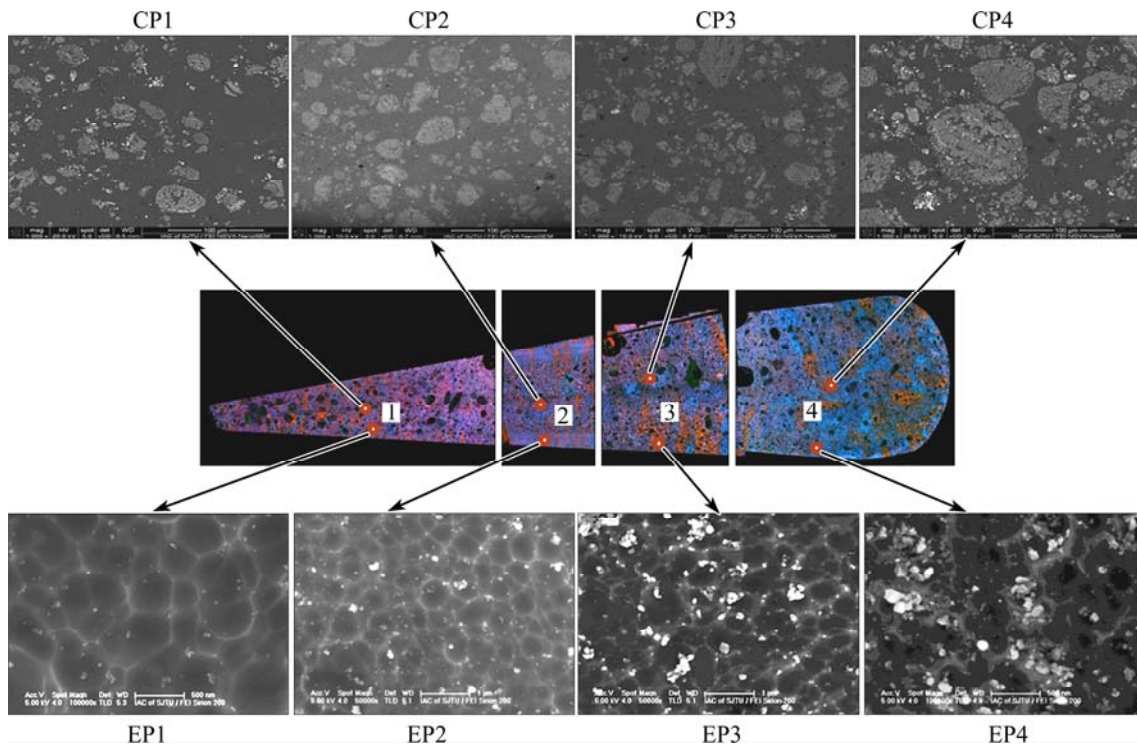


Fig. 2 Microstructures of wedge-shaped samples in different locations: 1—Sample 1; 2—Sample 2; 3—Sample 3; 4—Sample 4

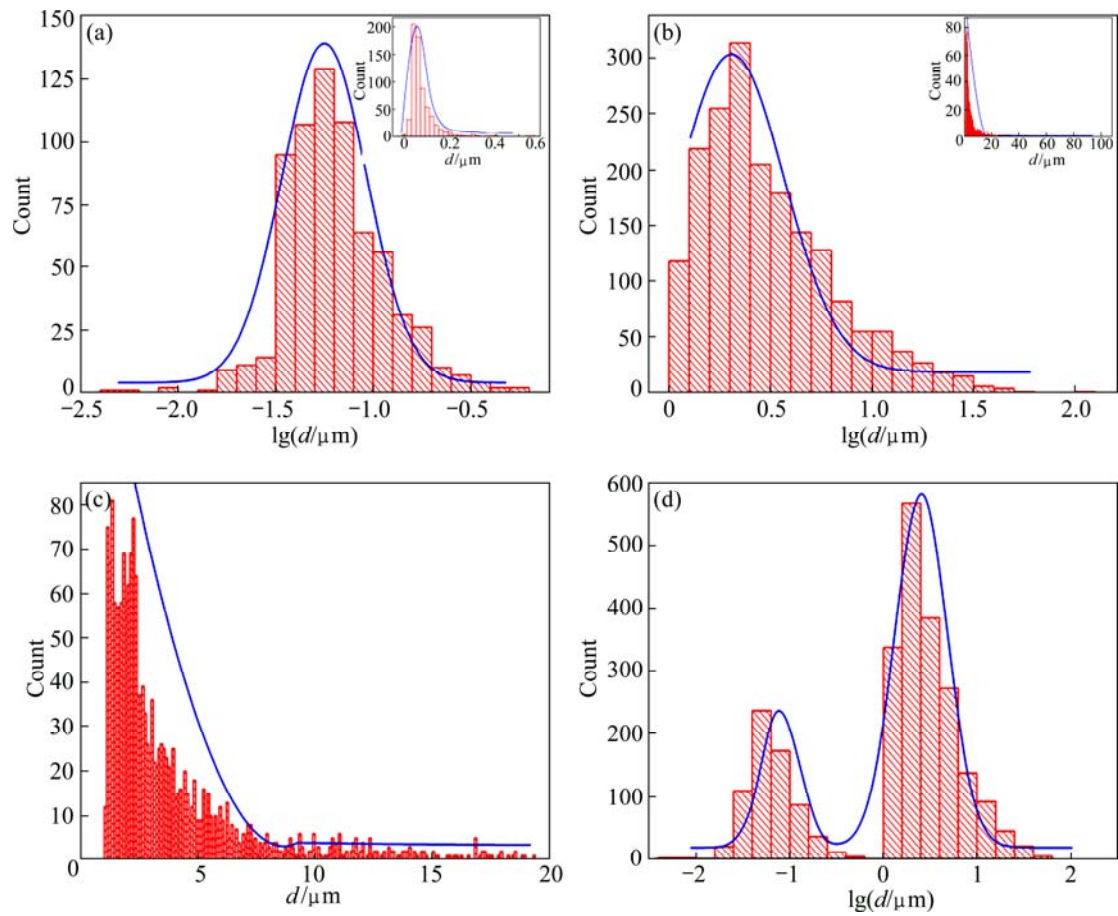


Fig. 3 Histogram and log-normal distribution in edge of wedge-shaped sample (a), histogram and log-normal distribution in center of wedge-shaped sample (b), local detailed view in center of wedge sample (c) and particle size distribution in whole wedge-cast sample (d)

Conversely, the standard deviation of 50.729 in the center of the wedge sample shows particles suffering serious reunion.

3.2 Measure of cluster degree

As stated above, the agglomeration of particles is more serious in the center of the wedge sample than that in the edge. In order to assess the aggregation degree in different locations of the wedge sample, the multi scale analysis of area fraction (MSAAF) [26] method is used in the present work. In this method, particles or clusters are extracted from a SEM microstructure image and then the extracted microstructure is divided into many quilts and each quilt square side length is Q , which changes from a single particle size to the full image size. A_f is the area fraction covered by the particles or the particle ensembles. Here, σ_{A_f}/A_f can be written in terms of localized area fraction statistics as:

$$\sigma_{A_f}/A_f = \left(\frac{\pi}{4A_f} \right)^{0.5} \left(\frac{Q}{d_p} \right)^{-1} \quad (4)$$

where d_p is the diameter of the particle or the cluster. It is evident that the selection of Q has a great impact on the value of σ_{A_f}/A_f ; meanwhile, it is easy to conclude from Eq. (4) that σ_{A_f}/A_f shows a linear relationship with Q/d_p in a logarithmic coordinate system and its slope is approximately -1 . Specific fitting curves of experimental data are illustrated in Fig. 4(b). The upper limit for σ_{A_f}/A_f shown by the broken line in Fig. 4(b) can be determined from the area fraction of the initial image, according to:

$$\sigma_{A_f}/A_f |_{Q/d_p \rightarrow 0} = \left(\frac{1-A_f}{A_f} \right)^{0.5} \quad (5)$$

Figure 4(a) schematically shows the image processing for the microstructure taken from the edge region of the wedge-cast sample. In Fig. 4(b), the red dots and the fitting line are based on the data gained from the samples in the edge of the wedge and the black dots and curves represent the data measured in the center of the wedge. This result leads to a parameter $L_{H(0.01)}/d_p$, the homogeneous length scale to be defined here, which is marked with small arrows on the horizontal axis evaluated at $\sigma_{A_f}/A_f = 0.01$. Here, a parameter f_c , cluster fraction, is introduced to quantitatively express the cluster degree in the wedge-cast sample. According to a certain A_f and $L_{H(0.01)}/d_p$, a certain f_c can be determined. The relationship between L_H , A_f and f_c can be gained from the previous work [26]. Combining L_H with A_f , it is easy to calculate that the cluster fraction, f_c , is about 0.2 and 0.6 in the edge and in the center of the sample, respectively.

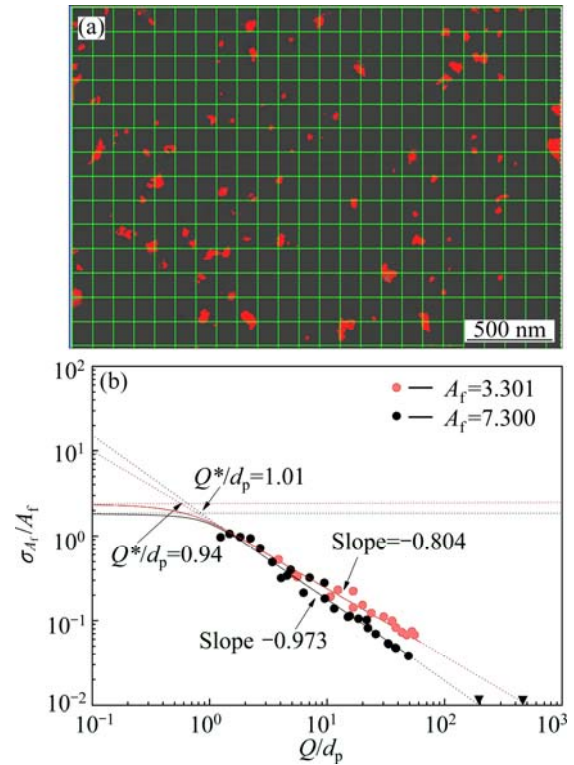


Fig. 4 Processing of particle extraction and grid in image chosen in edge of wedge sample (a) and MSAAF (multi scale analysis of area fraction) plots (b)

4 Discussion

In order to provide insight into the engulfment behavior of the particles or the clusters, it is necessary to focus on the solidification condition of the wedge-cast sample, as shown in Fig. 5, the wedge-shaped sample has a closely packed columnar grains microstructure near the wedge inclined surface and the growth direction is perpendicular to the surface. The columnar grains in this location are extremely fine, approximately $7 \mu\text{m}$ in the width, which does not allow the big clusters to be engulfed because of the fast cooling rate. It is also obvious in Fig. 5 that the columnar grains close to the copper mold are closely packed because the great temperature gradient will lead to heterogeneous nucleation on the copper surface easier and greater directional growth speed. Only a few of small particles can be engulfed at the interdendritic boundaries in the later stage of the solidification. This will contribute to the relatively uniform distribution of the particles near the cold copper mold surface. It is also noted that in the edge of the sample, solidification of the matrix appears to initiate primarily at the mold/sample interface almost simultaneously. Accordingly, the columnar grains originate from the nucleation on the copper mold and grow in an approximately parallel orientation towards the

center of the sample immediately. There is an obvious dividing line in the center of the mold, indicating that the columnar grain grows until the solidification fronts initiated on the opposite sides of the mold surface converged. The central portion of the wedge-shaped sample, however, is characterized by relatively coarse grains. This microstructure suggests that the solidification behavior of the wedge-shaped copper mold casting sample may deviate from the Newtonian fluid [27,28].

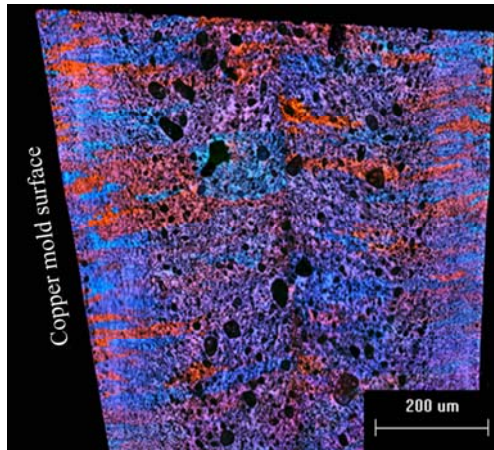


Fig. 5 Polarizing optical microstructure near cold copper mold surface

As mentioned previously, from sample 1 to sample 4, the degree of particle cluster increases but the tendency is not very intensive. The area percents of the particulates or clusters accounting for the matrix are 2.8%, 2.9%, 3.6% and 3.8% in the edge of the sample and 5.8%, 6.4%, 7.0% and 8.8% in the center of the sample for samples 1, 2, 3 and 4, respectively. In Fig. 2, the grains coarsen from sample 1 to sample 4 as the cooling rate decreases. In sample 1 and sample 2, the columnar grains in the edge of the sample are very fine, while in sample 3, the columnar grains are found easily but the grain size increases dramatically. In sample 4, there is no clear distribution of columnar grains and the microstructure of this portion is characterized by randomly oriented equiaxed grains. The results can explain the fact that the aligned columnar grains are unfavorable to the big cluster engulfment.

It should be noticed that the shape of the clusters examined in the scanning electron microscope is mostly round but their peripheries are irregular. That is evident when the cluster edge is extracted by the image analysis facility (Fig. 6(a)), compared with a single particle or the small clusters composed of few individual particles in the edge of the sample (Fig. 6(b)). The shape of the solidification front is convex, since the heat transfer coefficient of TiB_2 is far less than that of aluminum matrix. It is clear that the forces are symmetrical when a

perfectly smooth sphere interacts with the solid/liquid surface at one point. However, since a rough cluster contacts the solid/liquid surface in more than one point, the forces acting on the rough cluster are biased when the traditional formula for smooth particle is used for calculation.

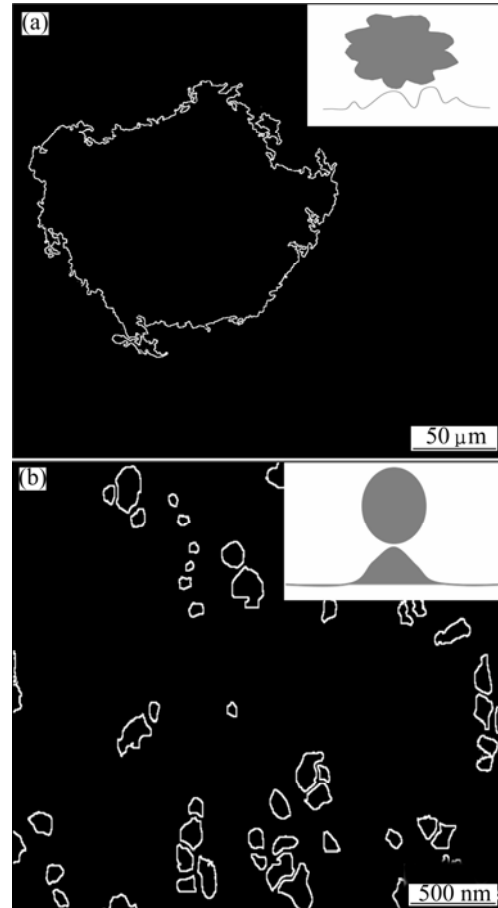


Fig. 6 Irregularities on periphery of clusters and contact of irregularities on periphery with solid/liquid surface (a), smooth margin of single particles and contact of smooth margin with solid/liquid surface (b)

Multipoint attachment between the clusters and the solid/liquid surface, schematically illustrated in Fig. 6(a), means less distorted solidification surface and less share of force developed at each point, compared with the total force required by single point of contact. UHLMANN et al [16] treated the case of irregularities on the surface of a spherical particle which reduces the effective radius and can hence lead to critical velocity considerably higher than that for comparable smooth particles. On the basis of the predecessors' work, in considering of the interface shape, viscous drag as well as the number of contact points, BOLLING and CISSE [17] expected that Eq. (6) can be used to calculate the critical velocity in the case of multipoint contact:

$$\eta^2 v^2 R^3 = N \Psi(\alpha)_{\max} \cdot 4kT\gamma\alpha_0 / (9\pi) \quad (6)$$

where η is the viscosity of the melt; v is the critical velocity; R is the radius of the particle or the cluster; N is the number of contact points; $\Psi(\alpha)$ is the function $\alpha(1-\alpha)^2(\alpha-\ln\alpha)$, α is a constant and $\alpha \leq 1$; k is the Boltzmann constant; γ is specific interfacial free energy and a_0 is the interatomic distance in the liquid. It is evident that the critical velocity v increases with the increase of the contact point N , as schematically shown in Fig. 6(a).

It should be noticed that the internal structure of the big clusters is skeleton framework-like, as shown in Fig. 7, which leads to the decrease of $\Delta\rho$ (the density difference between ceramic particle/cluster and Al melt). Fig. 7(b) shows that the space between the skeletons is about 1 μm . SURAPPA and ROHATGI [20] proposed that particle engulfment occurs when

$$\left(\frac{\lambda_p c_p \rho_p}{\lambda_l c_l \rho_l}\right)^{1/2} > 1 \quad (7)$$

where c is the specific heat capacity; λ is the heat coefficient; ρ is the density and subscript “p” and “l” refer to the particle and liquid, respectively. From Eq. (7), it is easy to conclude that the critical velocity $v \propto (\rho_p/\rho_l)^{-1}$

where ρ_p is always larger than ρ_l . In other words, the value of critical velocity is high for the skeleton framework clusters and the clusters are easy to be pushed when $\Delta\rho$ decreases as observed in the center of the wedge-shaped sample.

5 Conclusions

1) Cluster of TiB_2 particles in the aluminum matrix is serious in the wedge-cast sample. The overall tendency is that the size of particle clusters increases with the thickness of the wedge-shaped sample increasing.

2) The cluster degree of particles in the wedge sample is characterized by MSAAF method and the cluster fraction, f_c , is 0.2 and 0.6 in the edge and in the center of the wedge sample, respectively. The cluster diameter does not obey the normal distribution but approximately obeys the lognormal distribution in the edge and in the center of the wedge sample, respectively. But for the whole sample, the particle size obeys two separate log-normal distributions.

3) The big clusters are pushed by the solid/liquid front, and instead, the small particulates are engulfed in the edge of the sample. The most important is the neatly packed columnar grains close to the wedge inclined surface.

References

- [1] SAJJADI S A, EZATPOUR H R, PARIZI M T. Comparison of microstructure and mechanical properties of A356 aluminum alloy/ Al_2O_3 composites fabricated by stir and compo-casting processes [J]. *Mater Des*, 2012, 34: 106–111.
- [2] ARRABAL R, MINGO B, PARDO A. Pitting corrosion of rheocast A356 aluminium alloy in 3.5 wt.% NaCl solution [J]. *Corros Sci*, 2013, 73: 342–355.
- [3] KOCZAK M J. *Fundamentals of metal matrix composites* [M]. New York: Butterworth-Hermann, 1993.
- [4] SAJJADI S A, EZATPOUR H R, BEYGI H. Microstructure and mechanical properties of Al_2O_3 micro and nano composites fabricated by stir casting [J]. *Mater Sci Eng A*, 2011, 528(29): 8765–8771.
- [5] ZHANG Peng, LI Fu-guo. Effect of particle characteristics on deformation of particle reinforced metal matrix composites [J]. *Transactions of Nonferrous Metal Society of China*, 2010, 20(4): 655–661.
- [6] HE Long, TAN Ye-fe, TAN Hua. Tribological properties of nanostructured Al_2O_3 –40% TiO_2 multiphase ceramic particles reinforced Ni-based alloy composite coatings[J]. *Transactions of Nonferrous Metal Society of China*, 2013, 23: 2628–2627.
- [7] MAZAHERY A, SHABANI M O. Microstructural and abrasive wear properties of SiC reinforced aluminum-based composite produced by compocasting [J]. *Transactions of Nonferrous Metal Society of China*, 2013, 23(7): 1905–1914.
- [8] WATSONI G, FORSTER M F, LEE P D. Investigation of the clustering behavior of titanium diboride particles in aluminum [J]. *Compos: Part A*, 2005, 36: 1177–1187.
- [9] LUO Bin, SONG Xiao-jie, ZHANG Feng. Multi-functional thermosensitive composite microspheres with high magnetic

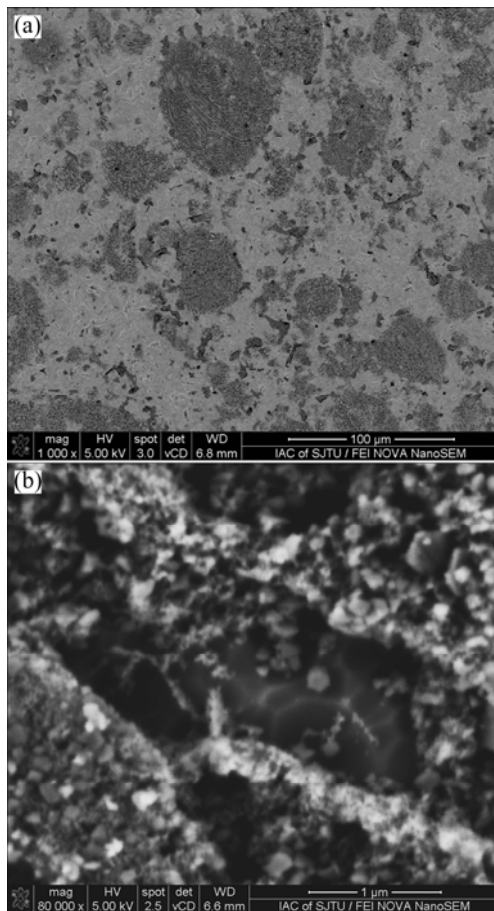


Fig. 7 Internal skeleton structure of clusters and morphology of the skeleton under low magnification (a) and high magnification (b)

- susceptibility based on magnetite colloidal nanoparticle clusters [J]. *Langmuir*, 2010, 26(3): 1674–1679.
- [10] TZZAMTZIS S, BAREKAR N S, BABU N H. Processing of advanced Al/SiC particulate metal matrix composites under intensive shearing—A novel phoe-process [J]. *Compos: Part A*, 2009, 40: 144–151.
- [11] NGUYEN V S, ROUXELD, HADJI R. Effect of ultrasonication and dispersion stability on the cluster size of alumina nanoscale particles in aqueous solutions [J]. *Ultrason Sonochem*, 2011, 18: 382–388.
- [12] LI Ping, ZHANG Xiang, XUE Ke-min, LI Xiao. Effect of equal channel angular pressing and torsion on SiC-particle distribution of SiC_p/Al composites [J]. *Transactions of Nonferrous Metal Society of China*, 2012, 22(S2): s402–s407.
- [13] DONG Pu-yun, ZHAO Hai-dong, CHEN Fei-fan, LI Jun-wen. Microstructures and properties of A356–10% SiC particle composite castings at different solidification pressures [J]. *Transactions of Nonferrous Metal Society of China*, 2013, 23(8): 2222–2228.
- [14] OMENYI S N, NEUMANN A W. Thermodynamic aspects of particle engulfment by solidifying melts [J]. *Appl Phys*, 1976, 47(9): 3956–3962.
- [15] YOUSSEF Y M, DASHWOOD R J, LEE P D. Effect of clustering particle pushing and solidification behavior in TiB₂ reinforced aluminum PMMCs [J]. *Compos: Part A*, 2005, 36: 747–763.
- [16] UHLMANN D R, CHALMERS B, JACKSON K A. The interaction between particles and a solid-liquid interface [J]. *Appl Phys*, 1964, 35: 2986–2993.
- [17] BOLLING G F, CISSE J. A theory for the interaction of particles with a solidifying front [J]. *Cryst Growth*, 1971, 10: 56–66.
- [18] STEFANESCU D M, DHINDAW B K, KRCAR S A, MOITRA A. Behavior of ceramic particles at the solid/liquid metal interface in metal matrix composite [J]. *Metall Trans A*, 1988, 19(11): 2847–2855.
- [19] KÖRBER Ch, RAU G. Interaction of particles and a moving ice-liquid interface [J]. *Cryst Growth*, 1985, 72: 649–662.
- [20] SURRAPA M K, ROHATGI P K. Preparation and properties of cast aluminium–ceramic particle composites [J]. *Mater Sci Lett*, 1981, 16(4): 983–993.
- [21] AGALLOTIS E, ROSENBERGER M R, SCHVEZOV C E. Numerical calculation of the drag force applied to particle pushing [J]. *Cryst Growth*, 2008, 310: 1366–1370.
- [22] HE Y, JAVAID A, ESSADIQI E. Numerical simulation and experimental study of the solidification of a wedge-shaped AZ31 MG alloy casting [J]. *Can Metall Quart*, 2009, 48(2): 145–155.
- [23] AGALLOTIS E M, SCHVEVOA C E, ROSENBERGER M R. A numerical model study of the effect of interface shape on particle pushing [J]. *Cryst Growth*, 2012, 354: 49–56.
- [24] PEREPEZKO J H, HILDAL K. Analysis of solidification microstructures during wedge-casting [J]. *Phill Mag*, 2006, 86: 3681–3701.
- [25] LI Peng-ting, LI Yun-guo, WU Yu-ying. Distribution of TiB₂ particles and its effect on the mechanical properties of A390 alloy [J]. *Mater Sci*, 2012, 546: 146–152.
- [26] SPOWART J E, MARUYAMA B, MIRACLE D B. Multi-scale characterization of spatially heterogeneous systems: Implication for discontinuously reinforced metal-matrix composite microstructure [J]. *Mater Sci*, 2001, 307: 51–66.
- [27] WU Y, LIU H, LAVERNIA E J. Solidification behavior of Al–Si/SiC MMCs, during wedge-mold casting [J]. *Acta Metal Mater*, 1994, 42: 825–837.
- [28] ZHANG Wen-ling, LIU Ying-dan, CHOI H J. Fabrication of semiconducting graphene oxide/polyaniline composite particles and their electrorheological response under an applied electric field [J]. *Carbon*, 2012, 50: 290–296.

TiB₂ 颗粒在楔形铜模铸锭中的分布以及吞噬行为

孙 靖, 张晓波, 蔡 庆, 张亦杰, 马乃恒, 王浩伟

上海交通大学 金属基复合材料国家重点实验室 上海 200240

摘 要: 通过楔形铜模铸造实验研究工业纯铝基体中 TiB₂ 颗粒的推移吞噬行为和颗粒或团聚体与液/固界面前沿之间的作用。实验结果表明: 在整个楔形试样中, 颗粒或团聚体的尺寸分别服从 2 个独立的分布, 团簇被推移到楔形试样的中间区域, 而单独的颗粒或小的团簇被楔形试样的边缘吞噬。在楔形试样的不同区域颗粒的团聚程度不同, 在试样的边缘和中间区域, 颗粒的团聚因子分别为 0.2 和 0.6。颗粒的直径并不服从一般的正态分布, 而是基本服从对数正态分布。更重要的是, 在整个试样中, 颗粒或团簇尺寸服从 2 个对数正态分布。

关键词: 非连续增强铝基复合材料; TiB₂; 楔形铜模铸造; 颗粒分布; 颗粒吞噬

(Edited by Yun-bin HE)